2022 IEEE International Conference on Robotics and Automation (ICRA)
May 23-27, 2022. Philadelphia, PA, USA

A Multi-VTOL Modular Aspect Ratio Reconfigurable Aerial Robot

Stephen J. Carlson, Prateek Arora, Christos Papachristos

***Abstract*— This work presents a novel Aspect Ratio-Modular Vertical Take-Off and Landing (ARM-VTOL) aerial robot, which is a meta-aircraft composed of two or more TiltRotor hybrid aircraft systems capable of magnetically being coupled during hovering flight, and of executing VTOL / Fixed-Wing hybrid missions once combined. The proposed meta-aircraft system carries the advantage of improved aerodynamic efficiency due its increased cumulative planform aspect ratio, which can be leveraged to achieve prolonged flight times in collaborative multi-vehicle flight. We propose an extendable methodology for its control which relies on the multi-body equivalent dynamics, and we present the coupling mechanism design that facilitates its experimental demonstration. We accompany these contributions with a field test-driven evaluation study conducted with a bi-vehicle ARM-VTOL prototype. The presented sequence includes vehicle-to-vehicle magnetic coupling during hovering flight, and is followed by a combined-vehicle mission comprising vertical climb, VTOL-forward transition, fixed-wing flight and maneuvering, and reverse-transition to VTOL and landing.**

I. INTRODUCTION

Aerial robotics continue to thrive, continuously expanding their real-world utility through technological breakthroughs in the intelligence, perception, and efficiency of autonomous flying systems. Small unmanned aircraft are increasingly encountered across intelligent remote sensing tasks [1–7], search and rescue [8–11], and even recently planetary exploration [12]. In this context of operational versatility, a consistent research theme has been trying to combine robotic modes of operation; reconfigurable Vertical Take-Off and Landing (VTOL) aircraft fall within this spectrum. The main trade-off required to achieve a viable hybrid aircraft platform is well established, namely the poor performance that a multi-flight-envelope design exhibits when compared to the maneuverability of traditional multirotors, or the endurance of fixed-wing aircraft, leaves the execution of real-world missions less efficient than desired. This work proposes a way to mitigate a class of aerodynamics-related limitations by proposing the ability to combine multiple hybrid VTOL vehicles into an elongated wing meta-aircraft, i.e. a novel Aspect Ratio-Modular VTOL (ARM-VTOL) aerial robot.

The proposed ARM-VTOL design considers a system-of-systems approach, with N wingtip-to-wingtip mechanically coupled TiltRotor aerial robots forming a semi-rigid planform. Hence, this novel meta-aircraft type possesses the ability to have a N-modular aerodynamic aspect ratio, standing to benefit from improved aerodynamic efficiency in forward-flight obtained as a result of minimized wingtip-induced losses. Our envisioned mode of operation relates to an autonomously organized swarm of hybrid Micro Aerial Vehicle robots, capable of autonomously combining themselves into a long-planform configuration in order to traverse longer distances than what the individual vehicle endurance would allow, and upon arrival disengage to resume any separately pursued objectives.

Fig. 1. The Aspect Ratio-Modular Vertical Take-Off and Landing (ARM-VTOL) reconfigurable aerial robot, consisting of a pair of wingtip-to-wingtip connected Tri-TiltRotor hybrid aircraft. Corresponding video available at: https://www.youtube.com/watch?v=pVbJudrOTGY

This work's contributions include: a) An analysis on the multi-body rotational and flight dynamics, leading to an extendable approach on how to control the proposed ARM-VTOL aircraft; b) The presentation of core system implementation aspects for a field deployable bi-vehicle ARM-VTOL prototype, accompanied by the detailed design of a novel wingtip-to-wingtip solid state magnetic coupling mechanism that accommodates an inter-system communication link which facilitates the deployed Master-Slave control topology; c) Field-proven experimental demonstration of the ARM-VTOL system viability with results and videos from a mission that includes vehicle-to-vehicle magnetic coupling during hovering, and is followed by a combined-vehicle automated mission comprising vertical climb, VTOL forward transition, fixed-wing flight and maneuvering, and reverse-transition to VTOL and landing.

The remainder of the paper is organized as follows: Section II presents related work. Section III describes modeling and control principles for the multi-body system, followed by Section IV which presents system design and implementation aspects. Section V demonstrates and discusses field test results. Conclusions are drawn in Section VI.

This material is based upon work supported by the NSF Award: AWD-01-00002751: RI: Small: Learning Resilient Autonomous Flight. The presented content and ideas are solely those of the authors.

The authors are with the University of Nevada, Reno, 1664 N. Virginia, 89557, Reno, NV, USA stephen_carlson@nevada.unr.edu

2022 IEEE International Conference on Robotics and Automation (ICRA) | 978-1-7281-9681-7/22/$31.00 ©2022 IEEE | DOI: 10.1109/ICRA46639.2022.9811542

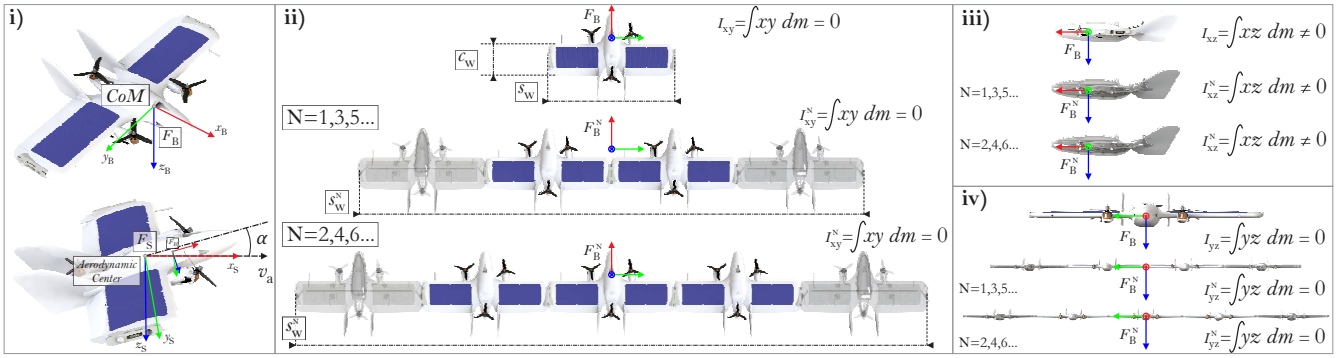

Fig. 2. i) Tri-TiltRotor single-vehicle reference frames definition. ii) N-vehicle Aspect-Ratio-Modular VTOL reference frames parametrized per odd / even-numbered configurations. Corresponding wing chord and cumulative planform length, which is the principle leveraged to achieve an increased Aspect Ratio aerial multi-robot platform in pursuit of its aerodynamic advantages. $ii) - iv$) Retained rotational symmetries per single-vehicle case (w.r.t. the elected reference frames) resulting in a similarly *structured* rigid body inertia tensor for the N-vehicle assembly.

II. RELATED WORK

Modular and Reconfigurable robotic systems, broadly introduced and treated in seminal works such as [13, 14], encompass a vast field of designs and applications. Specifically w.r.t. the field of aerial robotics, reconfigurable linking and composite formations have been illustrated in two subfields, namely the domain of multirotors, as well as the domain of fixed-wing aircraft [15]. In the multirotor space, a definitive archetype is the work related to the *Distributed Flight Array* [16–18]. Other relevant projects include [19–24]. Many of these use magnetic elements for binding flight elements together, and all address the dynamics and controllability of the respective compound hovering vehicle. Examples of multirotor arrays with variable frame geometry include [25–31]. However, none of these consider fixed-wing elements or control. In the fixed-wing space, aerial linking was studied seriously in early experiments with aerial refueling and range-extension for manned aircraft. The most notable experiment of this era was *Project TipTow*, as described in [32]. Recent studies in wingtip-to-wingtip linking are treated in [33–37], and notably in [38–40], with aircraft connected at the wingtips. The general case for meta-aircraft controllability in various configurations is treated in [41–43]. Pertinent and related to this are topics in aircraft controllability with highly-flexible wing geometry [44–47]; all aforementioned efforts remain theoretical investigations by nature however. To these authors' awareness, the most relevant records specifically about VTOL aircraft with wingtip-to-wingtip linking are found in [48–50]. These include patents that show relevant artwork, however it is unknown whether they are accompanied by real-world experiments.

III. PROPOSED APPROACH

This section details the considered aircraft class and our methodology in order to achieve an Aspect Ratio-Modular – Vertical Take-Off and Landing (ARM-VTOL) robotic platform by employing multiple reconfigurable MAV systems. More specifically, our approach departs from the standard Tri-TiltRotor (TTR) flying wing design [51, 52] and assumes an array of such aircraft serially and rigidly connected wingtip-to-wingtip such that they form a chain.

A. Modeling – Rigid Body Dynamics

We proceed to present the modeling approach of an ARM-VTOL which is composed as a modular chain of TTR aircraft with well-established dynamics in literature [53]. Figure 2 illustrates the employed choice of reference frames for different multi-body configurations, namely the Body Frame $\mathcal{F}_B^{\mathrm{N}}$, and the Stability Frame $\mathcal{F}_S^{\mathrm{N}}$. The Stability Frame is the native frame for expressing the aerodynamic forces, and its relationship to the Body Frame is $\mathcal{F}_B^{\mathrm{N}} = \mathbf{R}(\alpha)\mathcal{F}_S^{\mathrm{N}}$, where α the Angle-of-Attack (AoA) of the multi-wing assembly.

By this selection of reference frames, which relies on the N number of *identical* vehicles per configuration, $\mathcal{F}_B^{\mathrm{N}}$ is placed at the resulting assembly's Center-of-Mass (CoM). The body mass m scales as: $m^{\mathrm{N}} = \mathrm{N} \cdot m$. As shown in Figure 2, by having the aircraft conjoined at the wingtips, the resulting Moment of Inertia Tensor $\mathbf{I}^{\mathrm{N}}$ expressed w.r.t. $\mathcal{F}_B^{\mathrm{N}}$ maintains a similar structure to the single-vehicle case $\mathbf{I}$, i.e. it maintains the structural symmetries that zero-out its $\mathrm{I}_{xy}^{\mathrm{N}}$ and $\mathrm{I}_{yz}^{\mathrm{N}}$ products of inertia. The principal moments of inertia, and the non-zero product $\mathrm{I}_{xz}^{\mathrm{N}}$ for such a configuration, can be calculated using Steiner's theorem (for each N^{th} vehicle around $\mathcal{F}_B^{\mathrm{N}}$-aligned axes and combine them), as well as leveraging the assembly's xz-axial symmetry respectively:

$$\mathrm{N}: 1,3,5,\ldots \begin{cases} \mathrm{I}_{xx}^{\mathrm{N}} = \mathrm{N} \cdot \mathrm{I}_{xx} + 2m \sum_{n=2,4,6,\ldots}^{\mathrm{N}-1} n(\frac{s_w}{2})^2 \\ \mathrm{I}_{yy}^{\mathrm{N}} = \mathrm{N} \cdot \mathrm{I}_{yy} \\ \mathrm{I}_{zz}^{\mathrm{N}} = \mathrm{N} \cdot \mathrm{I}_{zz} + 2m \sum_{n=2,4,6,\ldots}^{\mathrm{N}-1} n(\frac{s_w}{2})^2 \\ \mathrm{I}_{xz}^{\mathrm{N}} = \sum_{n=1,2,3,\ldots}^{\mathrm{N}} - \int^m xz \; dm \; = \; \mathrm{N} \cdot \mathrm{I}_{xz} \end{cases} \tag{1}$$

$$\mathrm{N}: 2,4,6,\ldots \begin{cases} \mathrm{I}_{xx}^{\mathrm{N}} = \mathrm{N} \cdot \mathrm{I}_{xx} + 2m \sum_{n=1,3,5,\ldots}^{\mathrm{N}-1} n(\frac{s_w}{2})^2 \\ \mathrm{I}_{yy}^{\mathrm{N}} = \mathrm{N} \cdot \mathrm{I}_{yy} \\ \mathrm{I}_{zz}^{\mathrm{N}} = \mathrm{N} \cdot \mathrm{I}_{zz} + 2m \sum_{n=1,3,5,\ldots}^{\mathrm{N}-1} n(\frac{s_w}{2})^2 \\ \mathrm{I}_{xz}^{\mathrm{N}} = \sum_{n=1,2,3,\ldots}^{\mathrm{N}} - \int^m xz \; dm \; = \; \mathrm{N} \cdot \mathrm{I}_{xz} \end{cases} \tag{2}$$

where s_w the wing-span (tip-to-tip length) of a single vehicle.

These signify two important features, namely that a) the Newton-Euler formulated dynamics of the ARM-VTOL maintain a similar structure to [53], as well as b) the inertial values are parametrized w.r.t. the known single-vehicle ones.

B. Modeling – Aerodynamics

Aerodynamics modeling on the other hand requires to account for the modified downwash effects [54] achieved by chaining together N identical Flying-Wing aircraft. As shown in Figure 2, the total wing-span of the ARM-VTOL becomes $s_w^{\mathrm{N}} = \mathrm{N}s_w$, while the wing-chord c_w remains constant. This effectively increases the assembly's aerodynamic Aspect Ratio (AR), which is defined as $AR = \frac{{s_w}^2}{A_w}$, where A_w is the wing planform's $\mathcal{F}_{S_{xy}}^{\mathrm{N}}$-projected area. For the case of a near-rectangular planform, it becomes $AR \simeq \frac{s_w}{c_w}$, and therefore for the N-Flying Wing array $AR^{\mathrm{N}} \simeq \mathrm{N} \cdot AR$.

The pressure difference spillage around the wing-tips is known to induce a reduction of the free-stream aerodynamic lift coefficient C_{L_0} of an ideal infinite-wing by the rule: $C_L = C_{L_0}/(1 + \frac{C_{L_0}}{\pi \cdot AR})$. Therefore with a N-vehicle configuration we increase the effective lift coefficient by:

$$\frac{C_L^{\mathrm{N}}}{C_L}(\mathrm{N}) = \frac{\mathrm{N} \cdot (\lambda_1 + \lambda_2)}{\mathrm{N} \cdot \lambda_1 + \lambda_2}, \text{ where: } \lambda_1 = \pi \cdot AR \ , \ \lambda_2 = C_{L_0} \quad (3)$$

It is mentioned that for the induced drag coefficient C_D of a near-rectangular planform the corresponding relationship is $C_D = C_{D_0} + \frac{C_L^2}{0.7\pi \cdot AR}$, where C_{D_0} the ideal free-stream drag coefficient, which again makes possible the estimation of the factor that we affect the effective ARM-VTOL drag coefficient $\frac{C_D^{\mathrm{N}}}{C_D}(\mathrm{N})$ in known terms of the single Flying Wing:

$$\frac{C_D^{\mathrm{N}}}{C_D}(\mathrm{N}) = \frac{\mathrm{N} \cdot (\lambda_3 + \frac{C_L^{\mathrm{N}}}{C_L}(\mathrm{N}))}{\mathrm{N} \cdot \lambda_3 + 1}, \text{ where: } \lambda_3 = \frac{C_{D_0} 0.7\pi \cdot AR}{C_L^2} \quad (4)$$

Finally, Figure 3 shows the configuration of the wing control surfaces for the ARM-VTOL. Per the standard Flying Wing practice, these are employed as *elevons*, i.e. they serve the combined functionality of elevator and aileron. It is noted that the single aircraft strategy of assigning a "left" and "right" elevon based on their relative position w.r.t. the CoM is extended to the multi-vehicle assembly. Namely, for all N aircraft, each of their corresponding elevons' deflection angles are assigned as δ_{vl} if that lies on the left of the $\mathcal{F}_{S_{xz}}^{\mathrm{N}}$ plane, and as δ_{vr} otherwise. This directly retains the standard Flying Wing mixing relationship where a *virtual elevator* deflection angle δ_e is achieved via collective commanding, and a *virtual aileron* deflection angle δ_a via differential commanding respectively, i.e. for the ARM-VTOL:

$$\begin{bmatrix} \delta_e^{\mathrm{N}} \\ \delta_a^{\mathrm{N}} \end{bmatrix} = \begin{bmatrix} 1 & 1 \\ -1 & 1 \end{bmatrix} \begin{bmatrix} \delta_{vr}^{\mathrm{N}} \\ \delta_{vl}^{\mathrm{N}} \end{bmatrix} \ , \text{ where: } \begin{cases} \delta_{vr}^{\mathrm{N}}\text{: all } \delta^n \in \mathcal{F}_{S_y}^{\mathrm{N}} - \\ \delta_{vl}^{\mathrm{N}}\text{: all } \delta^n \in \mathcal{F}_{S_y}^{\mathrm{N}} + \end{cases} \quad (5)$$

These considerations signify another important feature, i.e. that one entire side of the assembly is equivalent to a *virtual left wing*, and the other side to a *virtual right wing*. Assuming the standard forces model for aerodynamic Lift F_L and Drag F_D [54], we obtain for the N-vehicle ARM-VTOL:

$$F_L^{\mathrm{N}} = \frac{1}{2}\rho v_a^2 \cdot A_w^{\mathrm{N}} \cdot C_L^{\mathrm{N}}(\delta_v) \quad , \quad F_D^{\mathrm{N}} = \frac{1}{2}\rho v_a^2 \cdot A_w^{\mathrm{N}} \cdot C_D^{\mathrm{N}}(\delta_v) \quad (6)$$

where ρ the air density and v_a the airspeed. It is highlighted that $A_w^{\mathrm{N}} = \mathrm{N} \cdot A_w$ is the cumulative planform area and $\{C_L^{\mathrm{N}}, C_D^{\mathrm{N}}\}$ are determined as shown in (3),(4). It is finally noted that the Lift and Drag coefficients characterize the aerodynamic profile and are functions of the *elevon* deflection angles; as all aircraft are identical and the $\{\delta_{vl}^{\mathrm{N}}, \delta_{vr}^{\mathrm{N}}\}$ are applied to the respective *left*-wing and *right*-wing assembly control surfaces uniformly, the corresponding $\{C_L(\delta_v), C_D(\delta_v)\}$ relationships remain unaffected in the N-vehicle case. Effectively, with our proposed ARM-VTOL we are increasing the length –and thus the Aspect Ratio– of the N-vehicle wings, while maintaining the aerodynamic profile.

C. Control

The control of the ARM-VTOL is considered w.r.t. the standard two modes of operation of a single TTR vehicle. Figure 3 illustrates the discussed formulations. We denote as $\{T_l, T_r, T_t\}$ the thrust generated by the left, right, and tail rotors, as $\{\gamma_l, \gamma_r\}$ the right and left rotor-tilt angles, and as $\{\boldsymbol{l}_f = [l_{f_x}, l_{f_y}], l_{t_x}\}$ the front and tail rotor moment arms.

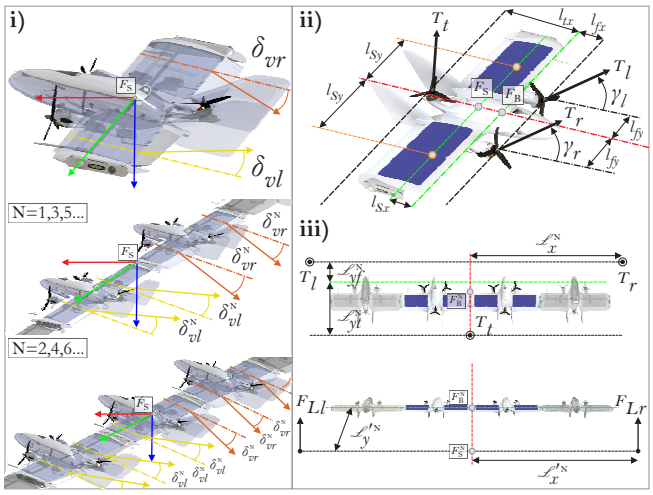

Fig. 3. *i*) Single-vehicle elevons and their mapping to the N-aircraft assembly, corresponding to a *virtual left wing* and *virtual right wing* of the resulting ARM-VTOL. *ii*) Definitions for thrust and rotor-tilt angles, as well as physical dimensions. Left / right wing aerodynamic centers denoted with orange. *iii*) N-vehicle scaled moment arms for thrust and lift forces; illustration of the employed equivalence of considering a scaled ARM-VTOL rigid body with a *virtual left*, *virtual right*, and *virtual tail*-side actuator (rotor / elevon) driven at the same value as the single-vehicle one.

In the *Helicopter* mode, aerodynamic effects are considered negligible, and the attitude actuation authority comes from generation of roll, pitch, yaw-controlling moments via left/right and front/tail differential thrusting, and left/right differential tilting for thrust-vectoring:

$$\begin{bmatrix} m_{B_x} \\ m_{B_y} \\ m_{B_z} \end{bmatrix} = \begin{bmatrix} \mathscr{L}_x(T_l \sin\gamma_l - T_r \sin\gamma_r) \\ \mathscr{L}_{y_f}(T_l \sin\gamma_l + T_r \sin\gamma_r) - \mathscr{L}_{y_t} T_t \\ \mathscr{L}_z(T_l \cos\gamma_l - T_r \cos\gamma_r) \end{bmatrix} \quad (7)$$

where $\mathscr{L}_x = l_{f_y}$, $\mathscr{L}_{y_f} = l_{f_x}$, $\mathscr{L}_{y_t} = l_{t_x}$, $\mathscr{L}_z = \sqrt{l_{f_x}^2 + l_{f_y}^2}\cos(\arctan\frac{l_{f_x}}{l_{f_y}})$, while for hovering force equilibrium the condition is $mg - T_r\sin\gamma_r - T_l\sin\gamma_l - T_t = 0$, where g the gravitational constant. For the N-vehicle configuration, we follow the approach of jointly treating actuator subsets as a *virtual left*, a *virtual right*, and a *virtual tail*-side rotor using the rule:

$$\begin{cases} \{T_l^{\mathrm{N}},\ \gamma_l^{\mathrm{N}}\}\text{: all } \{T^n,\ \gamma^n\} \in (\mathcal{F}_{B_x}^{\mathrm{N}} + \bigcap \mathcal{F}_{B_y}^{\mathrm{N}}-) \\ \{T_r^{\mathrm{N}},\ \gamma_r^{\mathrm{N}}\}\text{: all } \{T^n,\ \gamma^n\} \in (\mathcal{F}_{B_x}^{\mathrm{N}} + \bigcap \mathcal{F}_{B_y}^{\mathrm{N}}+) \\ T_t^{\mathrm{N}} \quad\ \text{: all } \{T^n,\ \gamma^n\} \in \mathcal{F}_{B_x}^{\mathrm{N}}- \end{cases} \tag{8}$$

i.e. left, right, and tail thrust values and tilt angles are uniformly applied to the corresponding single-vehicle actuators. By this strategy, we compute the N-vehicle equivalent scaled moment arms, i.e. the equivalent to assuming a single *collective left*, *right*, and *tail* actuator with their corresponding thrust (and rotor-tilt) values numerically the same as in (7).

$$\mathrm{N}: 1,3,5,\ldots \begin{cases} \mathscr{L}_x^{\mathrm{N}} = \mathscr{L}_x + \sum\limits_{n=2,4,6,\ldots}^{\mathrm{N}-1} n\cdot 2\frac{s_w}{2} \\ \mathscr{L}_{y_f}^{\mathrm{N}} = \mathrm{N}\cdot\mathscr{L}_{y_f} \\ \mathscr{L}_{y_t}^{\mathrm{N}} = \mathrm{N}\cdot\mathscr{L}_{y_t} \\ \mathscr{L}_z^{\mathrm{N}} = \mathscr{L}_z + \sum\limits_{n=2,4,6,\ldots}^{\mathrm{N}-1} (\mathscr{L}_z^{n,1} + \mathscr{L}_z^{n,2}) \end{cases} \tag{9}$$

$$\mathrm{N}: 2,4,6,\ldots \begin{cases} \mathscr{L}_x^{\mathrm{N}} = \sum\limits_{n=1,3,5,\ldots}^{\text{N-1}} n\cdot 2\frac{s_w}{2} \\ \mathscr{L}_{y_f}^{\mathrm{N}} = \mathrm{N}\cdot\mathscr{L}_{y_f} \\ \mathscr{L}_{y_t}^{\mathrm{N}} = \mathrm{N}\cdot\mathscr{L}_{y_t} \\ \mathscr{L}_z^{\mathrm{N}} = \sum\limits_{n=1,3,5,\ldots}^{\mathrm{N}-1} (\mathscr{L}_z^{n,1} + \mathscr{L}_z^{n,2}) \end{cases} \tag{10}$$

where $\mathscr{L}_z^{n,1} = \sqrt{l_{f_x}^2 + (l_{f_y}^{n,1})^2}\cos(\arctan\frac{l_{f_x}}{l_{f_y}^{n,1}})$ with $l_{f_y}^{n,1} = n\cdot\frac{s_w}{2} - l_{f_y}$, and $\mathscr{L}_z^{n,2} = \sqrt{l_{f_x}^2 + (l_{f_y}^{n,2})^2}\cos(\arctan\frac{l_{f_x}}{l_{f_y}^{n,2}})$ with $l_{f_y}^{n,2} = n\cdot\frac{s_w}{2} + l_{f_y}$. Together with (1),(2) we may therefore obtain an expectation of the relative scaling of attitude control moments versus rigid body inertia, parametrized w.r.t. the N number (and arrangement) of vehicles in the assembly. It is re-highlighted as per Section III-A that the rotational dynamics maintain the same structure, and with our strategy of collectively commanding actuator subsets as *virtual left*, *right*, and *tail* ones, we retain the single-vehicle Proportional-Derivative stabilizing controller synthesis [55] by scaling the gains by a constant factor based on the corresponding inertial –versus– moment arm ratio, to maintain the same net rotational acceleration. Regarding the ARM-VTOL's vertical hovering, it is straightforward that as long as each single vehicle lies at force equilibrium, using the strategy (8), the N-vehicle assembly also does.

In the *Fixed-Wing* mode, the single-aircraft attitude is controlled via the generation of aerodynamic-derived moments, and the specific control authorities are the elevator angle δ_e and aileron angle δ_a, which correspond to the pitch and roll control authority respectively. The aircraft yaw is controlled via coordinated roll-and-pitch commanding, i.e. the common banking-turn approach [56, 57]. The *Fixed-Wing* mode Proportional-Derivative controller is again assumed to be in place for each single-vehicle, and to provide the required stabilizing control which also enables its L_1 guidance [58]. The roll and pitch-controlling moments are:

$$\begin{bmatrix} m'_{B_x} \\ m'_{B_y} \end{bmatrix} = \begin{bmatrix} \mathscr{L}'_x(\cos\alpha(F_{Ll} - F_{Lr}) + \sin\alpha(F_{Dl} - F_{Dr})) \\ -\mathscr{L}'_y(\cos\alpha(F_{Ll} + F_{Lr}) + \sin\alpha(F_{Dl} + F_{Dr})) \end{bmatrix} \tag{11}$$

where the $\{l,r\}$-subscripted Lift and Drag forces correspond to the left and right wing contributions, $\mathscr{L}'_x = l_{S_y}$, $\mathscr{L}'_y = l_{S_x}$. As before, we compute the N-vehicle equivalent scaled moment arms using the (6) aerodynamic forces scaling:

$$\mathrm{N}: 1,3,5,\ldots \begin{cases} \mathscr{L}'^{\mathrm{N}}_x = \frac{\mathrm{N}\cdot(\lambda_1+\lambda_2)}{\mathrm{N}\cdot\lambda_1+\lambda_2}\cdot(\mathscr{L}'_x + \sum\limits_{n=2,4,6,\ldots}^{\mathrm{N}-1} n\cdot 2\frac{s_w}{2}) \\ \mathscr{L}'^{\mathrm{N}}_y = \frac{\mathrm{N}\cdot(\lambda_1+\lambda_2)}{\mathrm{N}\cdot\lambda_1+\lambda_2}\cdot\mathrm{N}\cdot\mathscr{L}'_y \end{cases} \tag{12}$$

$$\mathrm{N}: 2,4,6,\ldots \begin{cases} \mathscr{L}'^{\mathrm{N}}_x = \frac{\mathrm{N}\cdot(\lambda_1+\lambda_2)}{\mathrm{N}\cdot\lambda_1+\lambda_2}\cdot\sum\limits_{n=1,3,5,\ldots}^{\text{N-1}} n\cdot 2\frac{s_w}{2} \\ \mathscr{L}'^{\mathrm{N}}_y = \frac{\mathrm{N}\cdot(\lambda_1+\lambda_2)}{\mathrm{N}\cdot\lambda_1+\lambda_2}\cdot\mathrm{N}\cdot\mathscr{L}'_y \end{cases} \tag{13}$$

where the multiplicative first term comes from the increased Aspect Ratio's effect on the Lift coefficient per (3), while for brevity we omit terms corresponding to the effect on the Drag (4) as its moment contribution becomes comparatively much smaller for small Angles-of-Attack per (11).

As discussed, in the ARM-VTOL assembly there is uniform allocation of *virtual left wing* and *virtual right wing* elevon deflection angles, which per the (5) mapping determines a corresponding *virtual elevator* and *virtual aileron* $\{\delta_a^{\mathrm{N}}, \delta_e^{\mathrm{N}}\}$ that are used to command the N-vehicle attitude. Similarly as before, we utilize the scaled inertial –versus– moment arm ratios to scale the single-vehicle control synthesis gains to retain the net rotational accelerations across the controlled N-vehicle setup.

D. Discussion

Initially it is highlighted that the immediate advantage of employing this meta-aircraft approach comes from the aerodynamic efficiency gained via combining N-vehicle wings into a single planform, thus reducing by a factor of $\frac{1}{\mathrm{N}}$ the number of wingtips, which as mentioned are under the effect of pressure spillage. This implies a benefit stemming from a larger number aircraft; this is the reasoning behind the level of generalization in our accompanying analysis. Its results also however inform of the importance of appropriately adjusting the gain factors when the same (single-vehicle case) control synthesis is applied. For instance, while the pitch Degree of Freedom scaled inertia is similar across the *Helicopter* and *Fixed-Wing* modes, the equivalent moment arm becomes differently affected in the latter due to the increased aerodynamic lift efficiency terms. If one disregards this and applies a uniform scaling factor across the gains of both modes, the *Fixed-Wing* controller will be overtuned as a consequence and might lead to dangerous oscillatory

behavior during combined ARM-VTOL flight; it is noted that this has actually been our experimentally-verified experience.

IV. SYSTEM DESIGN

This section elaborates the design and implementation aspects of the proposed ARM-VTOL system. For the single-vehicle, we use the MiniHawk-VTOL [59, 60], which is a rapidly-prototyped aerial robotic platform. It is a 1 kg mass, 800 mm wingspan Tri-TiltRotor [61–66] with a typical cruising speed of 20 m/s. The aircraft's design accommodates solar-recharge capabilities and is focused on migratory aerial robotics research; yet its versatile 3D-printing fabrication enables its seamless adaptation as the individual vehicle basis for our proposed meta-aircraft VTOL.

A. Connection Mechanics

The MiniHawk-VTOL winglet was adapted with a specially designed solid-state magnetic coupler. This device contains an array of Neodymium magnets for initial alignment, capture and retention, as shown in Figure 4. Each coupler and its corresponding mate have peg-hole features for final alignment, which are optimized for shear-force-resistance and to keep the peg-hole connection phase-space as large as possible. It is noted that magnetic interaction between opposite coupler pairs very quickly centers the pegs before contact is made. The retaining force between couplers is 65 N face-to-face. A moment of 2 Nm in the normal (yaw) axis, and 1.6 Nm in the longitudinal (roll, or wing-bending) axis is required to break the connection. Through extensive experimental evaluation we validated that a firm connection is maintained during smooth flight, but also during challenging maneuvers for a bi-aircraft ARM-VTOL configuration.

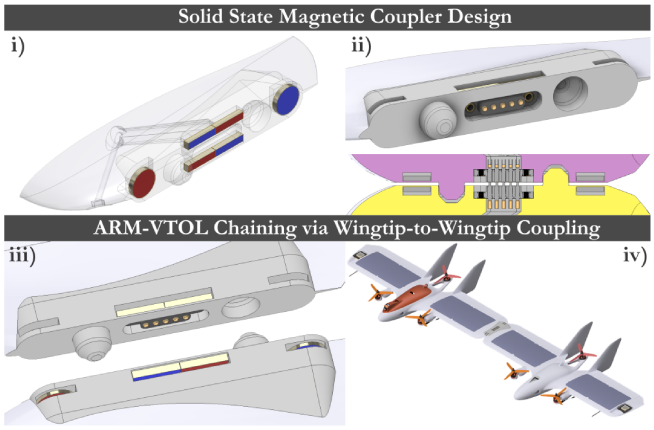

Fig. 4. i) Magnetic Coupler design, magnet layout and polarities (red: N, blue:S). ii) Peg-hole relationships and spring-loaded electrical contacts. iii) Coupler mating magnetic alignment. iv) Resulting wingtip-to-wingtip magnetically coupled bi-vehicle ARM-VTOL.

Finally, each coupler supports a set of spring-loaded pins and corresponding mating targets for a serial datalink between wingtip-to-wingtip coupled vehicles. Electrical connections between the couplers remain viable at up to 10 degrees of positive or negative longitudinal bend. Utilizing the UART transceivers on the flight controllers, a lightweight serial frame was designed for transferring setpoint and acknowledgment messages quickly, and with integrity checking. For typical operation, with a message cycle rate of 250 Hz at a baud rate of 921600bps, the link yields highly reliable behavior (less than 0.3% framing errors per 100,000 packets).

B. Multi–Aircraft Control

For the purposes of this work, we tackle the multi-vehicle control problem using a centralized approach. More specifically, one vehicle's autopilot is assumed to be the Master, while the other N − 1 aircraft act as Slaves. The Master flight controller is responsible for the execution of the stabilizing control policy and aerial robot guidance as per the single-vehicle control synthesis, but with the gain adaptation determined for the corresponding N-aircraft configuration. Effectively, this controller addresses the N-vehicle equivalent flight dynamics presented in the previous section, where the control actions correspond to a combination of *virtual left*, *virtual right*, and *virtual tail* rotor thrusts and tilt angles as well as a *virtual left wing* and *virtual right wing* elevon. The allocation policy is reflected by (8),(5), i.e. a simple distribution of the same set of values across all vehicles of the assembly. Therefore, the Master autopilot transmits the frame of setpoint values, and any Slave aircraft on the serial link directly forward these to their actuators.

It is noted that the Master autopilot needs to be aware of its position in the N-vehicle configuration, because any inertial values w.r.t. its own body frame $\mathcal{F}_B$ are required to be transformed by the ARM-VTOL frame $\mathcal{F}_B^{\text{N}}$.

The status of the mechanical wingtip-to-wingtip connection is inferred by the link quality; a consistent received sequence of valid (checksumed) setpoint frames received by the Slave enables its actuator-overriding policy. Additionally, the Slave replies with an acknowledgement message, thus appropriately informing the Master of its valid mechanical connection status. This is the necessary condition for the Master to also override its own scheduled control gains appropriately to account for operating as part of the N-vehicle assembly. In the event that this electro-mechanical link is separated, each flight controller independently reverts to apply its originally computed flight control actions.

It is mentioned that this policy does not offer a robust solution for recovery across all flight modes; rather it is the minimum viable one that enables the experimental demonstration and field testing of our proposed system implementation.

V. EXPERIMENTAL STUDY

We experimentally validated our proposed ARM-VTOL concept using a bi-vehicle configuration of two MiniHawk-VTOLs adapted with the presented magnetic coupler design at their wingtips. Figure 5 depicts corresponding key-instances of a field test conducted at the N. Nevada region. The sequence comprises four main phases, namely i) a separate single-vehicle Vertical Take-Off and mid-air coupling while hovering, ii) a combined ARM-VTOL ascent at 60 m Above Ground Level (AGL), iii) a Fixed-Wing loiter mission

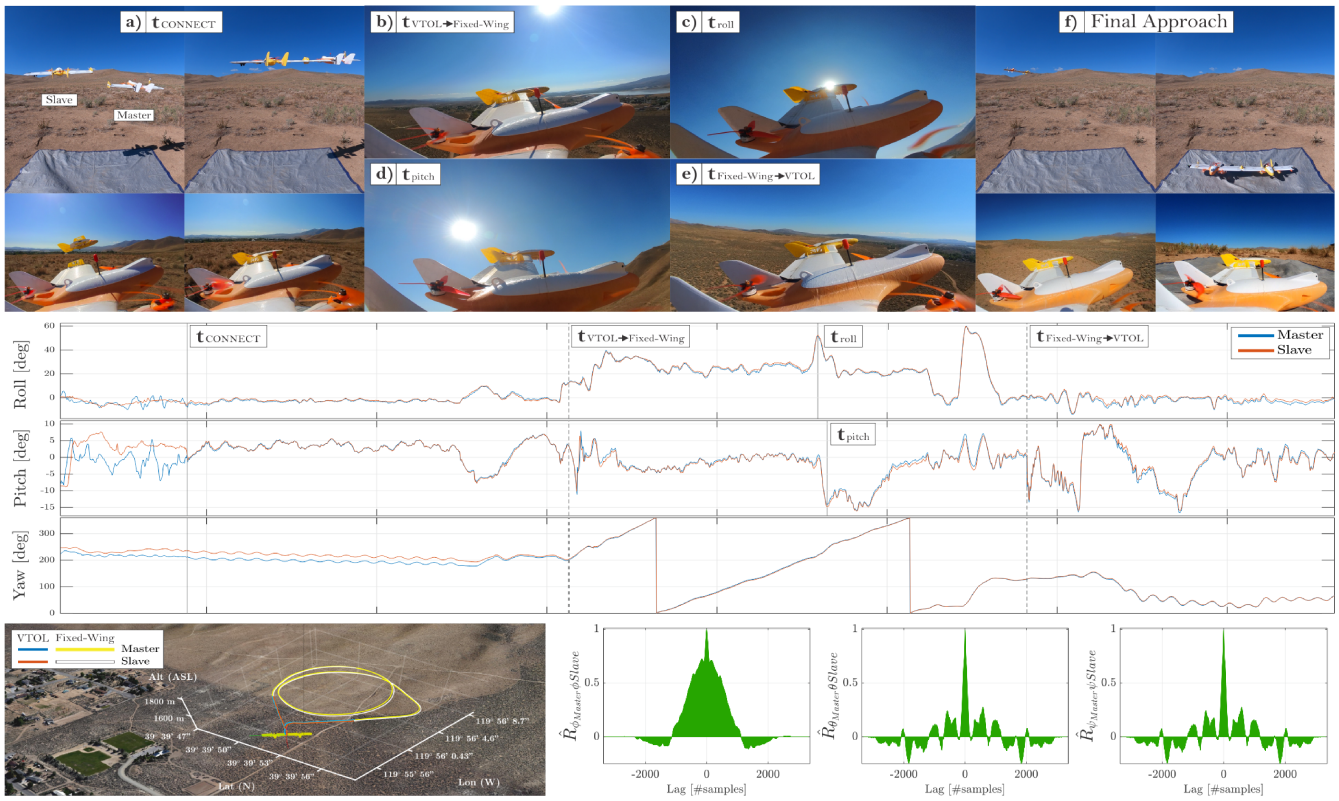

Fig. 5. *Top row*: a) Mid-air vehicle-to-vehicle connection (externally piloted) and initiation of combined ARM-VTOL autonomous waypoint mission. b) VTOL to Fixed-Wing transition, c) Steep roll during banking turn. d) Steep pitch during banking turn, e) Fixed-Wing to VTOL transition, f) Final approach and landing. *Mid row*: Corresponding rotational states of Master-&-Slave aircraft. *Bottom row*: Georeferenced trajectory of Master-&-Slave aircraft during mission. The VTOL and Fixed-Wing sections of the mission are color-coded differently for clarity. Master-*vs*-Slave cross-correlations of roll, pitch, and yaw validate the low-lag and high similarity rotational motion maintained during ARM-VTOL mission (post vehicle-to-vehicle magnetic coupling). Corresponding video available at: https://www.youtube.com/watch?v=pVbJudrOTGY

of 80 m radius, and finally iv) a VTOL landing back at the home location.

The initiating vehicle-to-vehicle coupling for the purposes of this paper is performed with the help of external guidance (human pilot visually guiding the Master aircraft's wingtip to "dock" into the Slave one which is performing Optical Flow-stabilized position hold). Apart from this "docking" sequence, the remainder of the mission is fully automated. In Figure 5, it can be observed that once the two aircraft become magnetically coupled, i.e. after $t_{CONNNECT}$ in the mid-row, their corresponding attitude states evolve smoothly together for the entire mission. Inspection of the corresponding time-series across the Master and Slave yields near-zero-mean sample lag and high correlation (corresponding subfigures are shown normalized for better overview). It is noted that regarding the yaw state, even though the two time-series take some time to converge in value, the signals remain highly correlated after the coupling occurs. This could potentially be attributed to the fact that yaw is inertially unobservable, and since the vehicles perform vertical ascent between $t_{CONNNECT}$ and $t_{VTOL \rightarrow Fixed-Wing}$, any strong local distortions of the Earth's magnetic field near the ground may be significantly reduced at that height.

These validate the effectiveness of our proposed approach, as the ARM-VTOL safely and smoothly executes the commanded $L1$ guidance maneuvers, driven by our Master-Slave scheme and supported by a mechanically simple yet effective coupling mechanism. Even more so, since it can be observed how across all challenging cases of: b) flight mode conversion into Fixed-Wing mode, c) heavy roll to execute a banking-turn, d) heavy pitch during a banking turn, e) flight mode conversion back to VTOL mode, the ARM-VTOL multi-body aircraft moves in near-perfect unison.

Finally, we provide a georeferenced overview of the presented ARM-VTOL field test and the corresponding mission footage as an accompanying video submission, where for clarity we separately color-code each autopilot's estimated flight path, as well as the part of the mission that corresponds to the vehicles operating in the VTOL and the Fixed-Wing mode respectively.

VI. CONCLUSIONS

In this work we presented a novel Aspect Ratio-Modular Vertical Take-Off and Landing aerial robot, i.e. a meta-aircraft composed of two or more TiltRotor VTOL systems capable of magnetically being coupled during hovering flight, and of executing VTOL–Fixed-Wing hybrid missions once combined. We analyzed the aerodynamic performance benefits of such a meta-robot, elaborated on an extendable methodology for its control, and presented the coupling mechanism design. The associated systems and methods are demonstrably validated via experimental field testing.

REFERENCES

[1] M. Burri, J. Nikolic, C. Hürzeler, G. Caprari, and R. Siegwart, "Aerial service robots for visual inspection of thermal power plant boiler systems," in *2012 2nd international conference on applied robotics for the power industry (CARPI)*. IEEE, 2012, pp. 70–75.

[2] S. Khattak, C. Papachristos, and K. Alexis, "Keyframe-based direct thermal–inertial odometry," in *2019 International Conference on Robotics and Automation (ICRA)*. IEEE, 2019, pp. 3563–3569.

[3] S. Khattak, C. Papachristos, and K. Alexis, "Keyframe-based thermal–inertial odometry," *Journal of Field Robotics*, vol. 37, no. 4, pp. 552–579, 2020.

[4] A. Bircher, K. Alexis, M. Burri, P. Oettershagen, S. Omari, T. Mantel and R. Siegwart, "Structural inspection path planning via iterative viewpoint resampling with application to aerial robotics," in *IEEE International Conference on Robotics and Automation (ICRA)*, May 2015, pp. 6423–6430. [Online]. Available: https://github.com/ethz-asl/StructuralInspectionPlanner

[5] T. Dang, F. Mascarich, S. Khattak, H. Nguyen, N. Khedekar, C. Papachristos, and K. Alexis, "Field-hardened robotic autonomy for subterranean exploration," *Field and Service Robotics (FSR)*, 2019.

[6] C. Papachristos, S. Khattak, and K. Alexis, "Uncertainty-aware receding horizon exploration and mapping using aerial robots," in *2017 IEEE international conference on robotics and automation (ICRA)*. IEEE, 2017, pp. 4568–4575.

[7] C. Papachristos, F. Mascarich, S. Khattak, T. Dang, and K. Alexis, "Localization uncertainty-aware autonomous exploration and mapping with aerial robots using receding horizon path-planning," *Autonomous Robots*, vol. 43, no. 8, pp. 2131–2161, 2019.

[8] N. Michael, S. Shen, K. Mohta, Y. Mulgaonkar, V. Kumar, K. Nagatani, Y. Okada, S. Kiribayashi, K. Otake, K. Yoshida *et al.*, "Collaborative mapping of an earthquake-damaged building via ground and aerial robots," *Journal of Field Robotics*, vol. 29, no. 5, pp. 832–841, 2012.

[9] M. Tranzatto, F. Mascarich, L. Bernreiter, C. Godinho, M. Camurri, S. M. K. Khattak, T. Dang, V. Reijgwart, J. Loeje, D. Wisth, S. Zimmermann, H. Nguyen, M. Fehr, L. Solanka, R. Buchanan, M. Bjelonic, N. Khedekar, M. Valceschini, F. Jenelten, M. Dharmadhikari, T. Homberger, P. De Petris, L. Wellhausen, M. Kulkarni, T. Miki, S. Hirsch, M. Montenegro, C. Papachristos, F. Tresoldi, J. Carius, G. Valsecchi, J. Lee, K. Meyer, X. Wu, J. Nieto, A. Smith, M. Hutter, R. Siegwart, M. Mueller, M. Fallon, and K. Alexis, "Cerberus: Autonomous legged and aerial robotic exploration in the tunnel and urban circuits of the darpa subterranean challenge," *Field Robotics*, 2021.

[10] T. Tomic, K. Schmid, P. Lutz, A. Domel, M. Kassecker, E. Mair, I. L. Grixa, F. Ruess, M. Suppa, and D. Burschka, "Toward a fully autonomous uav: Research platform for indoor and outdoor urban search and rescue," *IEEE robotics & automation magazine*, vol. 19, no. 3, pp. 46–56, 2012.

[11] P. Arora and C. Papachristos, "Mobile manipulationbased deployment of micro aerial robot scouts through constricted aperture-like ingress points," in *2021 IEEE/RSJ International Conference on Intelligent Robots and Systems (IROS)*, 2021, pp. 6716–6723.

[12] J. Balaram, M. Aung, and M. P. Golombek, "The ingenuity helicopter on the perseverance rover," *Space Science Reviews*, vol. 217, no. 4, pp. 1–11, 2021.

[13] K. Gilpin and D. Rus, "Modular robot systems," *IEEE robotics & automation magazine*, vol. 17, no. 3, pp. 38–55, 2010.

[14] K. Stoy, D. Brandt, D. J. Christensen, and D. Brandt, *Self-reconfigurable robots: an introduction*. Mit Press Cambridge, 2010.

[15] S. H. Derrouaoui, Y. Bouzid, M. Guiatni, and I. Dib, "A comprehensive review on reconfigurable drones: Classification, characteristics, design and control technologies," *Unmanned Systems*, pp. 1–27, 2021.

[16] R. Oung, A. Ramezani, and R. D'Andrea, "Feasibility of a distributed flight array," in *Proceedings of the 48h IEEE Conference on Decision and Control (CDC) held jointly with 2009 28th Chinese Control Conference*. IEEE, 2009, pp. 3038–3044.

[17] R. Oung and R. DAndrea, "The distributed flight array," *Mechatronics*, vol. 21, no. 6, pp. 908–917, 2011.

[18] R. Oung and R. DAndrea, "The distributed flight array: Design, implementation, and analysis of a modular vertical take-off and landing vehicle," *The International Journal of Robotics Research*, vol. 33, no. 3, pp. 375–400, 2014.

[19] D. Mellinger, M. Shomin, N. Michael, and V. Kumar, "Cooperative grasping and transport using multiple quadrotors," in *Distributed autonomous robotic systems*. Springer, 2013, pp. 545–558.

[20] D. Saldana, B. Gabrich, G. Li, M. Yim, and V. Kumar, "Modquad: The flying modular structure that self-assembles in midair," in *2018 IEEE International Conference on Robotics and Automation (ICRA)*. IEEE, 2018, pp. 691–698.

[21] D. Saldana, P. M. Gupta, and V. Kumar, "Design and control of aerial modules for inflight self-disassembly," *IEEE Robotics and Automation Letters*, vol. 4, no. 4, pp. 3410–3417, 2019.

[22] B. Gabrich, D. Saldana, and M. Yim, "Finding structure configurations for flying modular robots," *2021 IEEE/RSJ International Conference on Intelligent Robots and Systems*, 2021.

[23] B. Gabrich, D. Saldana, V. Kumar, and M. Yim, "A flying gripper based on cuboid modular robots," in *2018 IEEE International Conference on Robotics and Automation (ICRA)*. IEEE, 2018, pp. 7024–7030.

[24] Y. Litman, N. Gandhi, L. T. X. Phan, and D. Saldaña, "Vision-based self-assembly for modular multirotor structures," *IEEE Robotics and Automation Letters*, vol. 6, no. 2, pp. 2202–2208, 2021.

[25] M. Kulkarni, H. Nguyen, and K. Alexis, "The reconfigurable aerial robotic chain: Shape and motion planning," *IFAC-PapersOnLine*, vol. 53, no. 2, pp. 9295–9302, 2020.

[26] H. Nguyen, T. Dang, and K. Alexis, "The reconfigurable aerial robotic chain: Modeling and control," in *2020 IEEE International Conference on Robotics and Automation (ICRA)*. IEEE, 2020, pp. 5328–5334.

[27] S. H. Derrouaoui, Y. Bouzid, and M. Guiatni, "Nonlinear robust control of a new reconfigurable unmanned aerial vehicle," *Robotics*, vol. 10, no. 2, p. 76, 2021.

[28] F. Shi, M. Zhao, M. Murooka, K. Okada, and M. Inaba, "Aerial regrasping: Pivoting with transformable multilink aerial robot," in *2020 IEEE International Conference on Robotics and Automation (ICRA)*. IEEE, 2020, pp. 200–207.

[29] M. Zhao, T. Anzai, F. Shi, X. Chen, K. Okada, and M. Inaba, "Design, modeling, and control of an aerial robot dragon: A dual-rotor-embedded multilink robot with the ability of multi-degree-of-freedom aerial transformation," *IEEE Robotics and Automation Letters*, vol. 3, no. 2, pp. 1176–1183, 2018.

[30] M. Zhao, K. Kawasaki, T. Anzai, X. Chen, S. Noda, F. Shi, K. Okada, and M. Inaba, "Transformable multirotor with two-dimensional multilinks: Modeling, control, and whole-body aerial manipulation," *The International Journal of Robotics Research*, vol. 37, no. 9, pp. 1085–1112, 2018.

[31] D. Falanga, K. Kleber, S. Mintchev, D. Floreano, and D. Scaramuzza, "The foldable drone: A morphing quadrotor that can squeeze and fly," *IEEE Robotics and Automation Letters*, vol. 4, no. 2, pp. 209–216, 2018.

[32] C. Anderson, "Dangerous experiments: Wingtip coupling at 15,000 feet," *Flight Journal*, vol. 5, no. 6, p. 64, 2000.

[33] J. R. Cooper and P. M. Rothhaar, "Dynamics and control of in-flight wing tip docking," *Journal of Guidance, Control, and Dynamics*, vol. 41, no. 11, pp. 2327–2337, 2018.

[34] S. Magill, "Compound aircraft transport: Wing tip-docking compared to formation flight," Ph.D. dissertation, Ph. D. Dissertation, Dept. of Mechanical and Aerospace Engineering, Virginia , 2002.

[35] M. Wu, Z. Shi, T. Xiao, and H. Ang, "Effect of wingtip connection on the energy and flight endurance performance of solar aircraft," *Aerospace Science and Technology*, vol. 108, p. 106404, 2021.

[36] A. Puetz, A. O. Fares, J. Goldsberry, C. Navio, B. Kaiser, T. Bender, A. Denis, C. Kawagley, J. Markel, J. Martin *et al.*, "Unlinking of multiple autonomous, unmanned, aerial vehicles mid-flight," in *2018 AIAA Information Systems-AIAA Infotech@ Aerospace*, 2018, p. 0989.

[37] E. Levis, F. Pleho, and J. Hedges, "Viability of joined flight for small unmanned aerial vehicles," *The Aeronautical Journal*, vol. 124, no. 1273, pp. 297–322, 2020.

[38] C. Montalvo and M. Costello, "Meta aircraft connection dynamics," in *AIAA Guidance, Navigation, and Control Conference*, 2012, p. 4677.

[39] C. Carithers and C. Montalvo, "Experimental control of two connected fixed wing aircraft," *Aerospace*, vol. 5, no. 4, p. 113, 2018.

[40] M. Cobar and C. Montalvo, "Takeoff and landing of a wing-tip-connected meta aircraft with feedback control," *Journal of Aircraft*, pp. 1–10, 2021.

[41] C. Montalvo and M. Costello, "Meta aircraft flight dynamics," *Journal of Aircraft*, vol. 52, no. 1, pp. 107–115, 2015.

[42] S. Geuther, F. Capristan, J. Kirk, and R. Erhard, "A vtol small unmanned aircraft system to expand payload capabilities," *31st Congress of the International Council of the Aeronautical Sciences*, 2018.

[43] B. Troub and C. J. Montalvo, "Meta aircraft controllability," in *AIAA Atmospheric Flight Mechanics Conference*, 2016, p. 3395.

[44] C. Cesnik and W. Su, "Nonlinear aeroelastic simulation of x-hale: A very flexible uav," in *49th AIAA Aerospace Sciences Meeting Including the New Horizons Forum and Aerospace Exposition*, 2011, p. 1226.

[45] C. Cesnik and W. Su, "Nonlinear aeroelastic modeling and analysis of fully flexible aircraft," in *46th AIAA/ASME/ASCE/AHS/ASC Structures, Structural Dynamics and Materials Conference*, 2005, p. 2169.

[46] T. E. Noll, J. M. Brown, M. E. Perez-Davis, S. D. Ishmael, G. C. Tiffany, and M. Gaier, *Investigation of the helios prototype aircraft mishap volume i mishap report*. NASA, 2004.

[47] C. M. Shearer, "Coupled nonlinear flight dynamics, aeroelasticity, and control of very flexible aircraft." Ph.D. dissertation, University of Michigan, 2006.

[48] M. D. Patterson, J. Quinlan, W. J. Fredericks, E. Tse, and I. Bakhle, "A modular unmanned aerial system for missions requiring distributed aerial presence or payload delivery," in *55th AIAA Aerospace Sciences Meeting*, 2017, p. 0210.

[49] M. D. Patterson, J. R. Quinlan, and W. J. Fredericks, "Modular unmanned aerial system with multi-mode propulsion," Jan. 29 2019, US Patent 10,189,565.

[50] J. R. Quinlan and M. D. Patterson, "System and method for modular unmanned aerial system," Feb. 5 2019, US Patent 10,196,143.

[51] A. Bolsunovsky, N. Buzoverya, B. Gurevich, V. Denisov, A. Dunaevsky, L. Shkadov, O. Sonin, A. Udzhuhu, and J. Zhurihin, "Flying wingproblems and decisions," *Aircraft design*, vol. 4, no. 4, pp. 193–219, 2001.

[52] M. Tomac and G. Stenfelt, "Predictions of stability and control for a flying wing," *Aerospace Science and Technology*, vol. 39, pp. 179–186, 2014.

[53] J. A. Bautista, A. Osorio, and R. Lozano, "Modeling and analysis of a tricopter/flying-wing convertible uav with tilt-rotors," in *2017 International Conference on Unmanned Aircraft Systems (ICUAS)*. IEEE, 2017, pp. 672–681.

[65] C. Papachristos, K. Alexis, and A. Tzes, "Dual–authority thrust–vectoring of a tri–tiltrotor employing model predictive control," *Journal of intelligent & robotic systems*, vol. 81, no. 3-4, pp. 471–504, 2016.

[54] J. J. Bertin and R. M. Cummings, *Aerodynamics for engineers*. Cambridge University Press, 2021.

[55] F. Rinaldi, A. Gargioli, and F. Quagliotti, "Pid and lq regulation of a multirotor attitude: Mathematical modelling, simulations and experimental results," *Journal of Intelligent & Robotic Systems*, vol. 73, no. 1, pp. 33–50, 2014.

[56] T. R. Yechout, *Introduction to aircraft flight mechanics*. Aiaa, 2003.

[57] M. B. Tischler, *Advances in aircraft flight control*. CRC Press, 1996.

[58] S. Park, J. Deyst, and J. How, "A new nonlinear guidance logic for trajectory tracking," in *AIAA guidance, navigation, and control conference and exhibit*, 2004, p. 4900.

[59] S. J. Carlson and C. Papachristos, "The minihawk-vtol: Design, modeling, and experiments of a rapidly-prototyped tiltrotor uav," in *2021 International Conference on Unmanned Aircraft Systems (ICUAS)*. IEEE, 2021, pp. 777–786.

[60] S. J. Carlson and C. Papachristos, "Migratory behaviors, design principles, and experiments of a vtol uav for long-term autonomy," *ICRA 2021 Aerial Robotics Workshop on "Resilient and Long-Term Autonomy for Aerial Robotic Systems"*, 2021.

[61] C. Papachristos, K. Alexis, and A. Tzes, "Design and experimental attitude control of an unmanned tilt-rotor aerial vehicle," in *2011 15th International Conference on Advanced Robotics (ICAR)*. IEEE, 2011, pp. 465–470.

[62] C. Papachristos and A. Tzes, "Modeling and control simulation of an unmanned tilt tri-rotor aerial vehicle," in *2012 IEEE International Conference on Industrial Technology*. IEEE, 2012, pp. 840–845.

[63] C. Papachristos, K. Alexis, and A. Tzes, "Towards a high-end unmanned tri-tiltrotor: Design, modeling and hover control," in *2012 20th Mediterranean Conference on Control & Automation (MED)*. IEEE, 2012, pp. 1579–1584.

[64] C. Papachristos, K. Alexis, and A. Tzes, "Model predictive hovering-translation control of an unmanned tri-tiltrotor," in *2013 IEEE International Conference on Robotics and Automation*. IEEE, 2013, pp. 5425–5432.

[66] K. Alexis, C. Papachristos, R. Siegwart, and A. Tzes, "Robust model predictive flight control of unmanned rotorcrafts," *Journal of Intelligent & Robotic Systems*, vol. 81, no. 3-4, pp. 443–469, 2016.